Heliyon 5 (2019) e01972

Contents lists available at ScienceDirect

Heliyon

journal homepage: www.heliyon.com

Synthesis of sandwich-like Mn_3O_4@reduced graphene oxide nano-composites via modified Hummers' method and its application as uranyl adsorbents

Yingru Li *, Tao Gai, Lang Shao, Hao Tang, Rui Li, Shanli Yang, Shaofei Wang, Qian Wu, Yiming Ren **

Institute of Materials, Chinse Academy of Engineering Physics, Mianyang, Sichuan province, 621700, China

ARTICLE INFO

Keywords:
Materials science
Nuclear engineering
Graphene
Chemical processing
Uranyl adsorbents
Sandwich-like
Mn_3O_4@reduced graphene oxide nano-composites

ABSTRACT

Efficient and sustainable remediation technologies for uranium have recently been gaining more and more interest. Adsorption techniques are facile, effective and universal for kinds of heavy metal ions. In this paper, sandwich-like Mn_3O_4@reduced graphene oxide (Mn_3O_4@G) nano-composites were prepared facilely and greenly by adding NaOH solution into crude graphite oxide suspension prepared via the Hummers' method to modify the pH. The Mn_3O_4@G nanocomposites possess a reasonable maximum equilibrium adsorption quantity 195.6 mg [U] g^{-1}. Moreover, the magnetism of Mn_3O_4@G makes it easy to remove Mn_3O_4@G from water by strong magnet field.

1. Introduction

Uranium is the most abundant radioactive component in the nuclear wastes generated in nuclear industry, including uranium mining, production of uranium fuel, spent nuclear fuel reprocessing, etc [1, 2, 3, 4]. Given its strong toxicity and radioactivity, which are potential threatens of human health and eco-environment, the public concerns over nuclear accidents are arising with rapid development of nuclear industry, especially after Fukushima nuclear accident [5, 6]. Therefore, efficient and sustainable remediation technologies attract more and more interest. Sorption is a kind of facile, effective and universal removal technique for heavy metal ions. In natural environment, hexavalent uranium, namely uranyl (UO_2^{2+}) is the most common specie, and uranyl usually shows a strong tendency to be adsorbed onto some oxides like Fe_2O_3, SiO_2, etc [7, 8, 9, 10, 11, 12, 13]. Thus, developing highly efficient oxide absorbents is of crucial importance. Manganese oxides recently draw much attention, due to their low potential of zero charge, large specific surface area, rich negative charge, high surficial activity, etc [14, 15, 16, 17]. Remarkably, Mn_3O_4 nanoparticles, belonging to the spinel class of minerals with molecular formula of $Mn^{2+}(Mn^{3+})_2(O^{2-})_4$, shows special advantages for its unique magnetic properties among the manganese oxides family, allowing the facile and fast removal of the sorbents in a strong magnetic field after sorption procedure.

Typically, nano-filtration or high-speed centrifuge are involved to separate nanoparticles sorbents from the aqueous circumstance due to the strong Brown motion of the nanoparticles, which are not facile or economic. Chemical converted graphene (CCG) is a good carrier for nanoparticles for its one-atom-thick two-dimensional structure, high mechanical strength, large specific surface area and well chemical stability [18, 19]. However, the commercial applications of CCG have been limited by economic issues. CCG was usually synthesized via Hummers' or modified Hummers' method [20]. In these cases, graphene oxide (GO) aqueous dispersions contains a large quantity of impurities including Mn^{2+}, SO_4^{2-}, Cl^- ions, which need be purified. However, purification of GO dispersion is usually expensive and time-consuming, and requires a huge amount water (typically via dialysis, 1 kg GO needs about 10 ton of water in lab [20]). What is more, Mn^{2+}, considered as soluble impurity in Hummers' method and a kind of heavy metal pollution, is actually the precursor of kinds of functional manganese oxide materials mentioned above. The removal of Mn^{2+} is not only uneconomical or a threaten to the eco-environment, but also a waste of valuable Mn resource. Thus, it is of important scientific meaning and potential industrial value to simplify

* Corresponding author.
** Corresponding author.
E-mail addresses: liyingru@caep.cn (Y. Li), renyiming@caep.cn (Y. Ren).

https://doi.org/10.1016/j.heliyon.2019.e01972
Received 18 September 2018; Received in revised form 9 April 2019; Accepted 17 June 2019

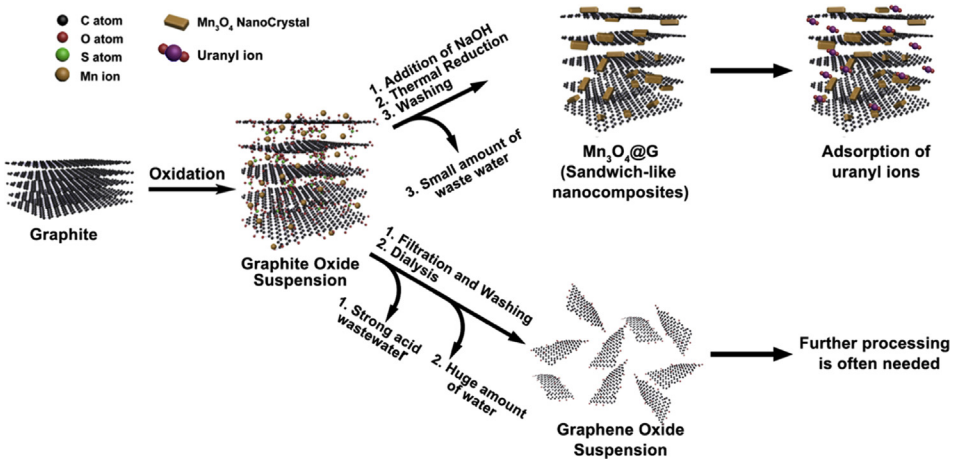

Fig. 1. Illustration of the preparation of Mn_3O_4@G.

the purification procedure of GO and develop novel methods to utilize these Mn resources.

In this work, via changing the traditional after treatments in Hummers' method, we have developed a novel method to synthesize a new-type composite of Mn_3O_4 and reduced graphene oxide named as Mn_3O_4@G. The Mn_3O_4@G possesses a unique sandwich-like structure: Mn_3O_4 nanoparticles intercalate between the graphene sheets. More importantly, the Mn_3O_4@G could be utilized as adsorbents for uranyl ions with reasonable adsorption capacity (195.6 mg [U]/g). Moreover, the magnetism of Mn_3O_4 could help to separate the sorbent, Mn_3O_4@G, from the bulk solution efficiently in magnetic field.

2. Experimental

2.1. Materials and solution

Natural graphite powders were purchased from Alfa Aesar (325 mesh). $KMnO_4$, H_2SO_4, H_2O_2, HCl, NaOH and NaCl were bought from Sinopharm Chemical Reagent Co. Ltd. (Shanghai, China). Uranyl nitrate was provided by Dingtian Chem. Corp (Xi'an, China). The uranyl nitrate solution was prepared via dissolving uranyl nitrate in de-ionic water. The uranium concentration of the parent solution was controlled around 200 mg L^{-1} and the testing solution was prepared by diluting it. The pH of the uranyl nitrate solution was adjusted by NaOH and HCl, and the ionic strength was adjusted by NaCl.

2.2. Synthesis of sandwich-like Mn_3O_4@G nanocomposites

The synthesis procedures of the sandwich-like Mn_3O_4@G nanocomposites are illustrated in Fig. 1. Firstly, crude graphite oxide was synthesized by oxidizing natural graphite powders via a modified Hummers method. The detailed procedures are described as below: Graphite powders (3 g) were added to concentrated sulfuric acid (70 mL, 1.26 mol) under stirring with ice-water bath; under vigorous agitation, potassium permanganate (12.0 g) was added slowly to ensure that the temperature of the mixture is below 5 °C; after the mixture is homogeneous, the reaction system was transferred to a 40 ± 5 °C water bath and stirred for 2 h, resulting in a thick dark brown paste; then, 200 mL deionic water was added and followed by a slow addition of 50 mL H_2O_2 (30%), and the color of the solution turned from dark brown to bright yellow, implying that residual MnO_4^- had transferred into Mn^{2+}; thus, the crude graphite oxide suspension containing a large amount of Mn^{2+} was finally obtained.

Secondly, after the suspension cooling down to room temperature, NaOH solution (500 mL 6 M, meaning the amount of NaOH is 3 mol) was added to the suspension slowly and carefully with cool water bath, to avoid the boiling of the suspension. At last, the color of the suspension changed from bright yellow to black. Then, the black suspension was transferred in to an oven under 120 °C to evaporate the water. Successively, the temperature of the oven was raised to 170 °C for 4 h to thermal reduce the GO sheets.

Finally, the black solid consisting of the nanocomposites together with alkali and salt impurities was re-dispersed in de-ionic water. After filtration and washing by de-ionic water to remove the residual alkali and salt impurities, dark brown powders which were the sandwich-like Mn_3O_4@G nanocomposites final products were obtained.

2.3. Synthesis of contrast materials

In order to fully investigate the structure of Mn_3O_4@G, Mn_3O_4 nanoparticles, GO and directly thermal reduced graphene oxide (dtRGO) were also synthesized. In the meanwhile, a sample of Mn_3O_4@G was treated by concentrated HCl solution to remove the Mn_3O_4, and the final product without Mn_3O_4 is named as G. The Mn_3O_4 nanoparticles were synthesized from $MnCl_2$ and NaOH referring to [21], The detail of preparing the abovementioned materials are listed below.

Synthesis of GO solid: the crude graphite oxide suspension obtained in Section 2.2 was filtered and washed with 1:4 HCl aqueous solution (400 mL) to remove Mn^{2+} ions followed by washing with 400 mL water to remove the acid. The resulting solid was then diluted in deionic water. Then, the suspension was purified by dialysis for one week using a dialysis membrane with a molecular weight cut off of 8,000 to 14,000 Da to remove the residual metal species and other impurities. The obtained dark brown suspension was subjected to 30 min of centrifugation at 4000 rpm to remove any aggregates and then 30 min of centrifugation at 10,000 rpm to remove liquid containing small pieces of grapheme. Finally, the purified GO suspension was freezing dried, and yellow foam-like solid was obtained.

Synthesis of dtRGO: the dtRGO was prepared via thermal treatment of GO sample at 700 °C for 4 h with a heating rate of 10 °C under Ar atmosphere in a tube furnace (GSL 1700X, Hefei Kejing, China).

Synthesis of G: the Mn_3O_4@G powders (1 g) were dispersed in concentrated HCl solution (20 mL) overnight, and successively filtered and washed by deionic water. The filtering flake was then dried under 80 °C in an oven, and black powders were obtained finally.

2.4. Characterizations

Scanning electron microscope (SEM) images were obtained by a JSM-6480A microscope (Japan Electronics). Transmission electron microscope (TEM) images were taken on a JEM-2010 microscope (JEM-2010, Japan) with an accelerating voltage of 120 kV. The X-ray diffractograms

(XRD) from a Bruker D8 Advance diffractometer (Bruker, USA). The samples were also analyzed with a Raman microscope with 512 nm laser excitation (Horba JobinYvon, France), FT-IR spectrometer (Bruker Vertex 70) and X-ray photoelectron spectroscopy (XPS) (Thermo Fisher Scientific, USA) operating with Al-Kα radiation. The N_2 absorption-desorption isotherms of the samples were tested with liquid nitrogen (78 K) adsorption by the Brunauer-Emmet-Teller method (Autosorb iQ Station 2, Quantachrome Instruments, U.S.A.). The thermogravimetry analyses were performed on a simultaneous thermal analyzer (Netzsch STA 449F3, Germany).

2.5. Adsorption tests

(1) Isotherm

In a batch experiment, 1 mg of the Mn_3O_4@G was added into 5 mL uranyl nitrate solution in a plastic centrifuge tube. The adsorption was undertaken in a water-bath shaker under constant temperature of 25 °C for 8 h to achieve adsorption equilibrium. After the adsorption, the tubes were centrifuged to precipitate the Mn_3O_4@G powders and the supernatant solution was analyzed using a UV-Vis spectrometer (Shimazu, UV-Vis 1800) at 651.5 nm in the presence of Arsenazo III (a complexing agent) to obtain the concentration of uranyl ion. The amount of uranium being adsorbed was calculated according to Eq. (1):

$$Q_e = \frac{(C_0 - C_e)V}{m} \quad \text{Eq. (1)}$$

where Q_e refers to the equilibrium adsorption capacity, C_0 and C_e represent the initial and equilibrium uranium concentrations, respectively, V is the total volume (i. e. 5 mL), and m is the absorbent mass (i. e. 1 mg).

(2) Adsorption rate

200 mg of the Mn_3O_4@G was added into 1 L uranyl nitrate solution ([U] = 31.2 mg mL^{-1}, pH = 5, I = 0.01 M) in a plastic bottle. The adsorption was undertaken in a water-bath shaker under constant temperature of 25 °C. A series of samples (2 mL) were taken at a series of time by injectors with filter heads. And then the concentrations were measured by UV-Vis spectra to calculated the adsorption quantity.

(3) Regeneration

200 mg of the Mn_3O_4@G was added into 1 L uranyl nitrate solution ([U] = 31.2 mg L^{-1}, pH = 5, I = 0.01 M) in a plastic bottle. The adsorption was undertaken in a water-bath shaker under constant temperature of 25 °C for 8 h to ensure adsorption equilibrium. After adsorption, the suspension was filtered to separate the Mn_3O_4@G powders. The uranyl concentration filtrate was then measured by UV-Vis spectra to calculated the adsorption quantity. The filter cake of Mn_3O_4@G was then washed by diluted HNO_3 solution (pH = 3) repeatedly. The regenerated Mn_3O_4@G was added into another one litre of uranyl nitrate solution ([U] = 31.2 mg L^{-1}, pH = 5, I = 0.01 M), and repeat the adsorption experiment.

3. Results & discussion

3.1. Synthesis advantages

The procedures of preparing Mn_3O_4@G nanocomposites are schematically illustrated in Fig. 1. In this method, the oxidization procedure shows no differences with the tradition Hummers' method, except for the detailed ratio of raw material. The key change is the sufficient addition of NaOH into the crude GO suspension after oxidization. A large quantity of Mn^{2+} ions are absorbed or intercalated between the graphene sheets. As

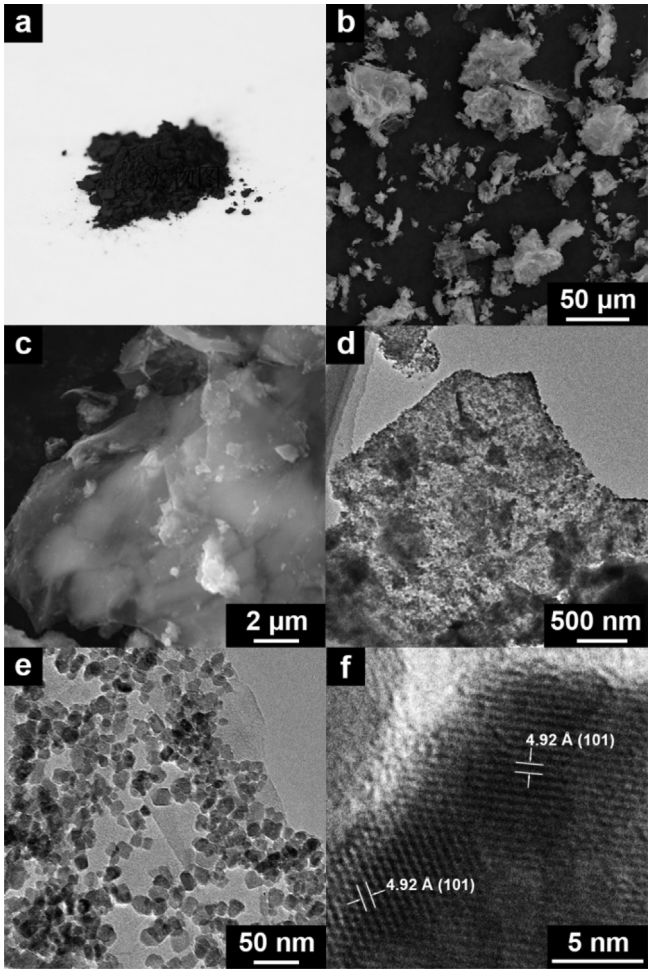

Fig. 2. a) Photograph of Mn_3O_4@G; b, c) SEM images of Mn_3O_4@G with different magnifications; d, e, f) TEM images of Mn_3O_4@G with different magnifications.

the pH value changes, the Mn^{2+} ions in the crude graphite oxide suspension, usually regarded as waste or impurity and need be removed before further application, are transferred into Mn_3O_4 nanoparticles on the surface of graphene sheets according to the following chemical reactions (1), (2) [22]. As a consequence, we have fully utilized the raw material to achieve higher atom economy.

$$4Mn^{2+} + 8OH^- + O_2 \rightarrow 4MnOOH + 2H_2O \quad (1)$$

$$12MnOOH \triangleq 4Mn_3O_4 + 6H_2O + O_2 \uparrow \quad (2)$$

Moreover, the crude graphite oxide does not need the sonication, centrifugation, or dialysis processes usually involved in Hummers method for exfoliation and purification of GO before thermal reduction. In the washing procedure, since the hydrophilic GO has turned into hydrophobic RGO, the gelation of GO is avoided, and the coordination to impurity metal ions of the oxygen-containing groups on the GO sheets disappears. Thus, the water dosage could be reduced. Typically, in traditional synthesis route, to fabricate 1 g GO material will produce 10 kg acidic wastewater in lab. Meanwhile, to fabricate 1 g Mn_3O_4@G will only produce less than 200 g slightly alkaline wastewater. Thus, our method is more simple, cheaper, atom-economic and eco-friendly than those reported previously.

3.2. Morphology and structure

In macroscopic view, the Mn_3O_4@G powders appears dark brown,

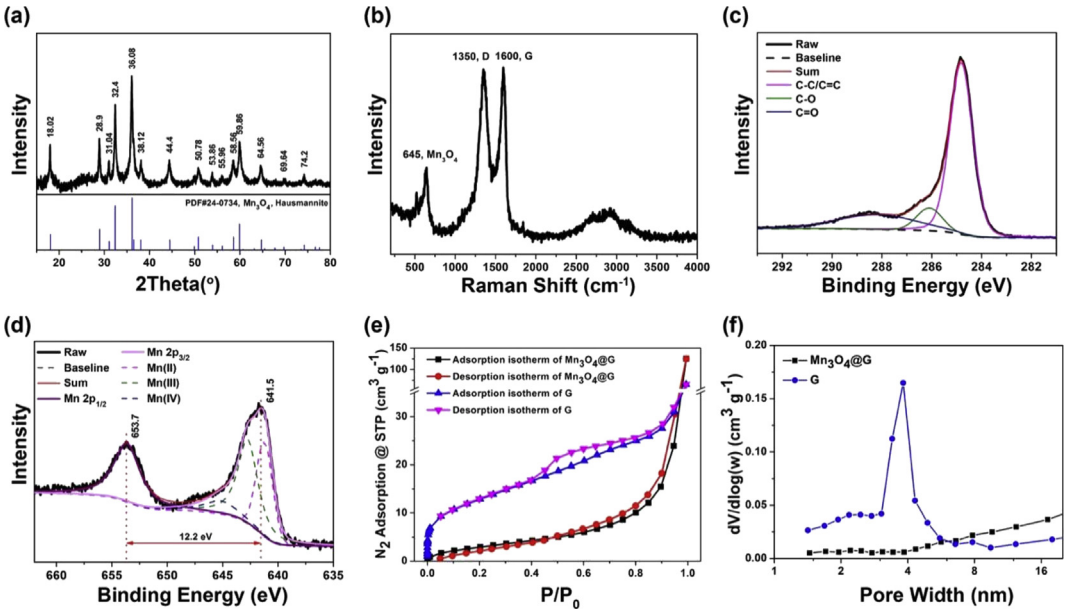

Fig. 3. Characterizations of Mn_3O_4@G: a) XRD patterns, b) Raman spectrum, c) C1s XPS curve, d) Mn2p XPS curve, e) N_2 adsorption-desorption isotherm of Mn_3O_4@G and G, f) pore width distribution Mn_3O_4@G and G based on (e).

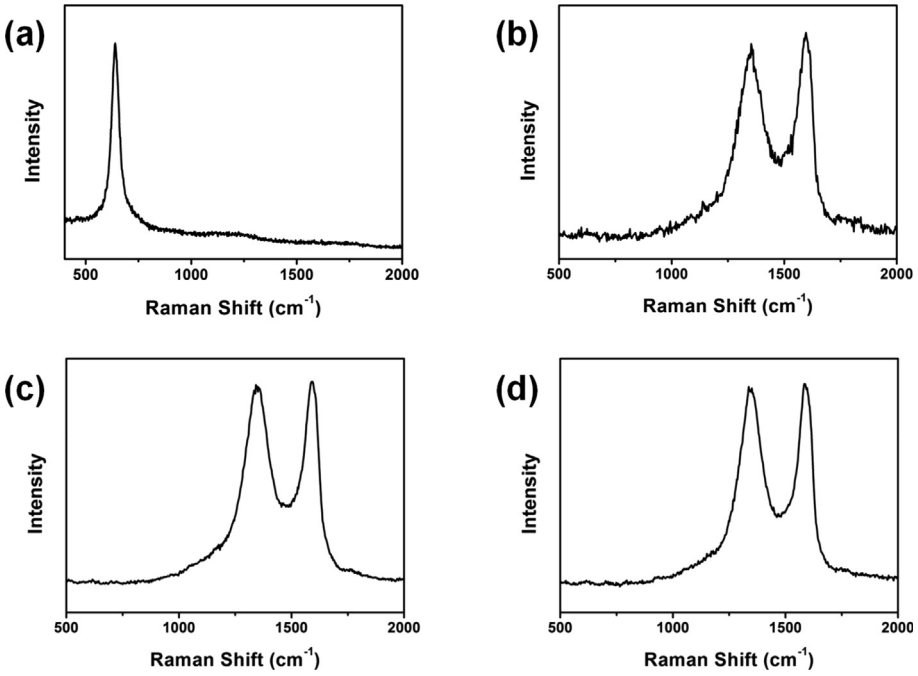

Fig. 4. Raman spectra of a) Mn_3O_4 nanoparticles, b) GO, c) dtRGO, and d) G.

which is the colour of Mn_3O_4 rather than graphene material (Fig. 2a). In SEM images, the Mn_3O_4@G powders are irregular particles, possessing typical laminar graphene layers with the size ranging from several micrometres to tens of micrometres (Fig. 2b). High-resolution SEM image shows that these graphene sheets are partially exfoliated, while no large cracks or holes between graphene layers could be observed (Fig. 2c). This mainly comes from the inhibition effect of NaOH on the gas release during the thermal treatment: excessive NaOH could react with the gaseous decomposition products of crude GO like CO_2 and SO_x, inhibiting the dramatic expansion caused by releasing gas. In the TEM images (Fig. 2d, e), Mn_3O_4 nanoparticles uniformly distributed on the surface of RGO sheets with the size of 10–30 nm. By etching the nanoparticles using concentrated HCl solution, the mass fraction of Mn_3O_4 nanoparticles is measured to be about 68.2 %, and the mass fraction of the remaining reduced graphene oxide is 31.8 %. In the high resolution TEM images, a clear crystalline structure of Mn_3O_4 was observed (Fig. 2f), whose lattice fringes with a lattice spacing of 4.92 Å agree well with the (101) crystal planes of Mn_3O_4 [17].

3.3. *Chemical structures*

The XRD patterns of Mn_3O_4@G show sharp and intense peaks assigned to the lattice plane of typical Mn_3O_4 crystal (PDF#24–0734), and besides, no obvious peaks related to other manganese oxide are

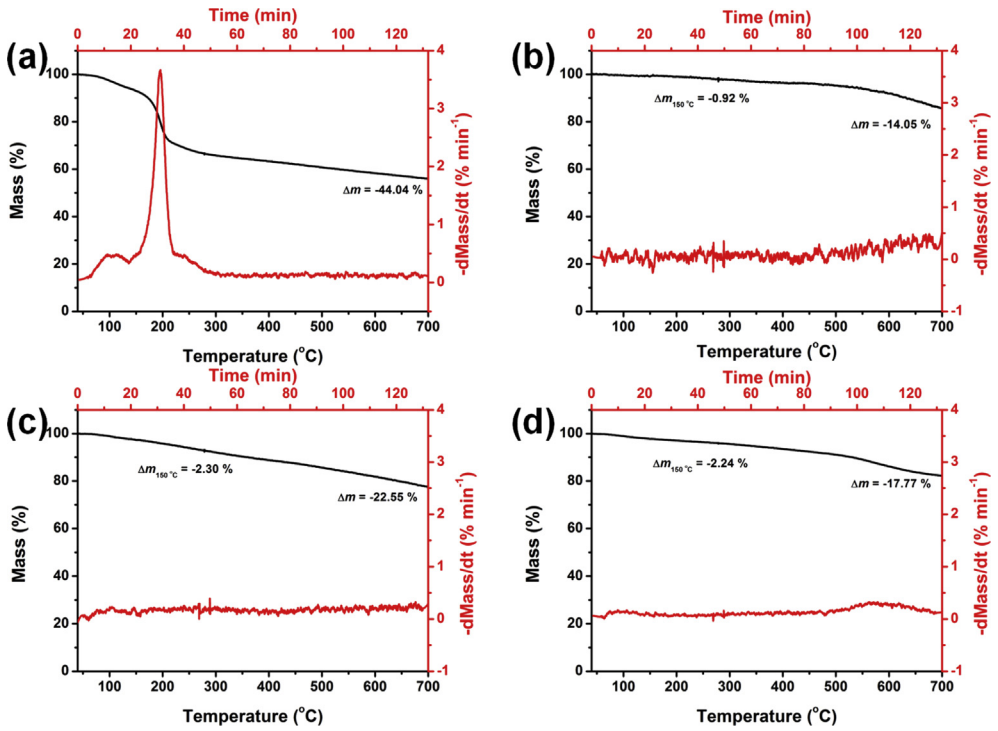

Fig. 5. TGA and dTGA curves of a)GO, b) dtRGO, c) G, and d) Mn_3O_4@G.

observed, meaning that a highly crystalline Mn_3O_4 is successfully synthesized (Fig. 3a).

In order to fully study the chemical structure of Mn_3O_4@G, the Raman spectra of Mn_3O_4@G and the corresponding materials including synthesized Mn_3O_4 particles, GO, dtRGO and G were studied. The Raman spectrum of Mn_3O_4@G show two groups of characteristic peaks assigned to RGO and Mn_3O_4 respectively (Fig. 3b). The band at about 645 cm^{-1} is associated with the tetragonal spinel structure of Mn_3O_4, agreeing with the Raman spectrum of the pure synthesized Mn_3O_4 particles very well (Fig. 4a), which is the characteristic peak of all the spinel structures, like Fe_3O_4. It is assigned to the A1g mode, relating to the Mn–O breathing vibration of Mn^{2+} in tetrahedral coordination [17, 23]. Moreover, the characteristic peak of Mn_3O_4 disappears in the Raman spectrum of G, meaning that all Mn_3O_4 nanoparticles have been removed. Two remarkable bands at about 1350 and 1600 cm^{-1} assigned to the D- and G-bands of carbon occur in all graphene-containing materials (Mn_3O_4@G, GO, dtRGO, and G; Fig. 3b, Fig. 4b,c,d). The G-band is related to graphitic carbons, while D-band is associated with either structural defects or partially disordered structures. The intensity ratio of D-band and G-band (I_D/I_G) reflects the structural integrity. The I_D/I_G value of GO is calculated to be about 0.90, and that of dtRGO is calculated to be about 0.98. The increase of the I_D/I_G value implies the GO sheets were reduced and the conjugated structures were partially restored during the thermal treatment [20, 24]. Furthermore, theI_D/I_G values of dtRGO, Mn_3O_4@G and G are similar, although the temperature of the thermal treatment during fabricating Mn_3O_4@G is 170 °C, much lower than that of preparing dtRGO (700 °C). Thus, these results suggests that the RGO sheets in Mn_3O_4@G and dtRGO should share similar reduction degree.

Moreover, the thermogravimetry analysis (TGA) and differential thermogravimetry analysis (dTGA) curves of GO, G (the etched sample), dtRGO and Mn_3O_4@G not only confirm that the GO sheets have been reduced partially, but also provide more information about the chemical structures of these materials (Fig. 5). In TGA curves, the weight losses around 100 °C should be contributed from the releasing of trapped water and the weight loss of GO is significantly higher than the others, indicating a higher content of water in GO because of its more hydrophilic

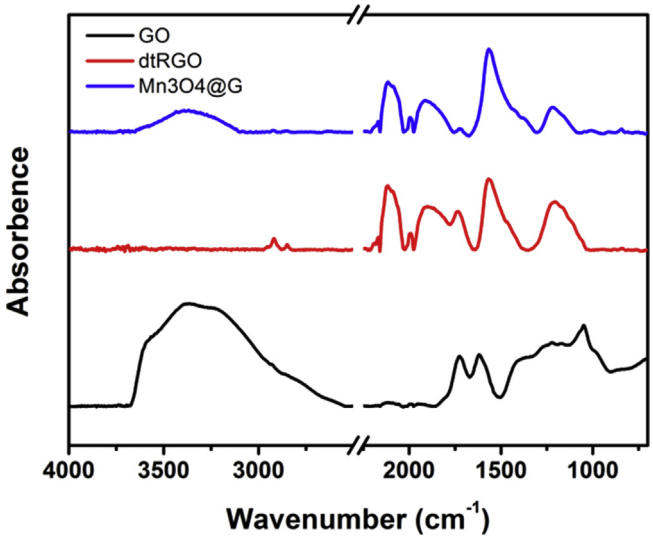

Fig. 6. The FTIR spectra of GO, dtRGO and Mn_3O_4@G.

oxygenated groups. The sharp weight loss of GO between 130 and 220 °C is attributed to the decomposition of less stable oxygen containing functional groups on GO sheets, while the curves of dtRGO, G and Mn_3O_4@G do not show this phenomenon [20]. The shoulder peak observed around 240 °C in the dTGA curves of GO does not appear in other materials either, which is associated with the sulfate or sulfuric acid impurities. The TGA curves of dtRGO and G both exhibit steady and nearly-linear decreases after 100 °C. Nevertheless, the slope for G is larger than that for dtRGO, and the final mass losses of G and dtRGO are 22.55 % and 14.05 %, respectively, indicating a larger oxygen content in G. Thus, it can be inferred that the thermal treatment at 170 °C for 4 h is enough to remove most of the less stable oxygen containing functional groups on GO sheets, however, some more stable oxygen containing functional groups remains. In addition, the dTGA curve of Mn_3O_4@G

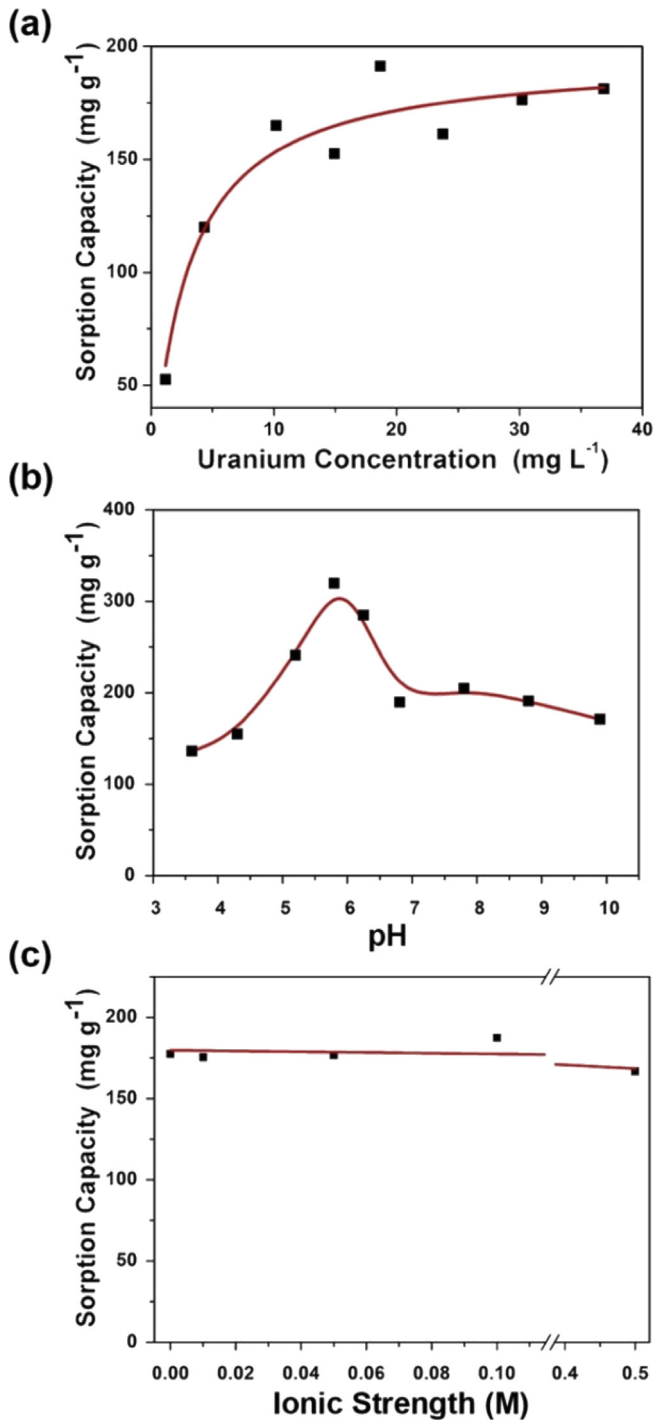

Fig. 7. The adsorption properties of Mn_3O_4@G towards uranyl ions: a) the isotherm at 298 K, pH = 5.0 and [I] = 0.01 M; b, c) impact of pH and ionic strength on the adsorption capacity, respectively (T = 298 K [U] = 37.6 mg L^{-1}).

shows a broad peak from 550 °C to 650 °C, which does not appear in other simple graphene materials without manganese oxide. It might be attributed to the degradation from Mn_3O_4 to MnO, and the released oxygen would react with graphene sheets rapidly.

The FTIR analysis demonstrate the differences of the functional groups on the graphene sheets of GO, dtRGO and Mn_3O_4@G (Fig. 6). The most remarkable change of the FTIR curves from GO to either dtRGO or Mn_3O_4@G is the weakening of the broad peak at the high-wavenumber region, which is associated to stretching vibration of O–H. The broad

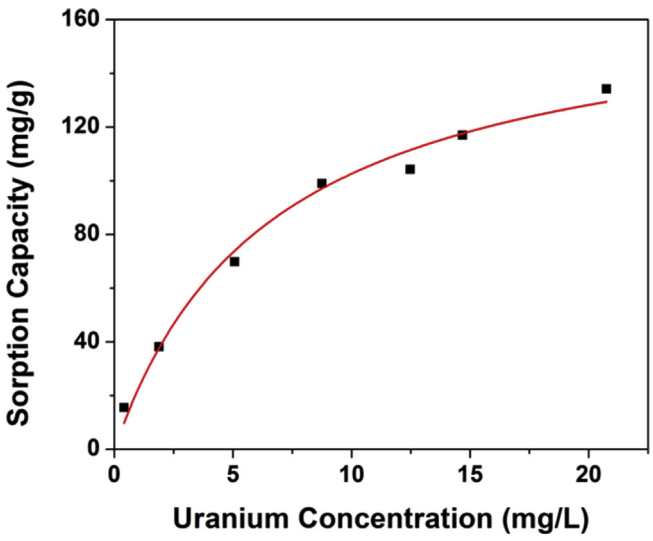

Fig. 8. The adsorption isotherm of synthesized Mn_3O_4 powders towards uranyl ions at 298 K, pH = 5.0 and [I] = 0.01 M.

peak disappears in the FTIR curve of dtRGO, and still remains a rather small peak for Mn_3O_4@G. Combining the results of TGA, it also confirms that most hydrophilic oxygen containing groups on the graphene sheets of Mn_3O_4@G have been removed, and only a small amount of thermal stable groups still remains. The peaks at 1610 cm^{-1} associated to stretching vibration of C=C of the dtRGO and Mn_3O_4@G curves are both strengthened in comparison with that of GO. Moreover, new peak at about 2200 cm^{-1} appears in both the dtRGO and Mn_3O_4@G curves, which should be contributed from the cumulative double bond and triple bond of carbons. It should be noted here that the generation of the cumulative double bond and triple bond of carbons will certainly result in disorders in the graphene lattice, leading the strengthen of the D-band in Raman spectra. These results agree very well with the above Raman and TGA results, that the graphene sheets of Mn_3O_4@G are partially reduced. And now it can be concluded that the properties of graphene sheets in Mn_3O_4@G should be closer to dtRGO rather than GO.

The XPS analysis provides the information of elements' valence state. The C1s XPS demonstrate the presence of three types of carbon bonds: C–C/C=C (284.8 eV), C–O (286.2 eV), and C=O (288.4 eV) (Fig. 3c). The bands associated oxygen-containing groups are much weaker than that associated with C–C/C=C band, suggesting that most of the oxygen-containing groups are removed and the conjugated domains are partially restored, agreeing with the above analyses. The Mn2p XPS also confirms the existence of Mn_3O_4 (Fig. 3d). The $Mn2p_{3/2}$ peak is centered at 641.5 eV and the $Mn2p_{1/2}$ peak at 653.7 eV, with a splitting of 12.2 eV, agreeing with the reported values for Mn_3O_4 earlier [17]. The $Mn2p_{3/2}$ peak can be separated into three Gaussian functions and the simulative peaks locate at 640.9, 642.8 and 645.1 eV. The peak at 640.9 eV drives from Mn (II), while that at 642.8 eV from Mn (III), reflecting the chemical structure of Mn_3O_4. The weak peak at 645.1 eV representing Mn (IV) should originate from surficial oxidation state of the Mn_3O_4 nanoparticles.

To further identify the location of the Mn_3O_4 nanoparticles inside the graphene sheets, the N_2 adsorption experiments of Mn_3O_4@G and G were performed. The adsorption isotherm of Mn_3O_4@G (Fig. 3e) exhibits a Type-III isotherm with a tiny increase in the low relative pressure intensity region, and its desorption isotherm does not possess an obvious hysteresis loop, suggesting that Mn_3O_4@G nanoparticles do not have obvious micropores or mesopores. The specific surface area (SSA) is calculated to be 12.31 m^2 g^{-1}. However, the isotherm of G changed dramatically as the Mn3O4 nanoparticles have been removed (Fig. 3e). A larger increase appears at the initial stage of the adsorption isotherm, indicating the formation of micropores. Moreover, the SSA of G is

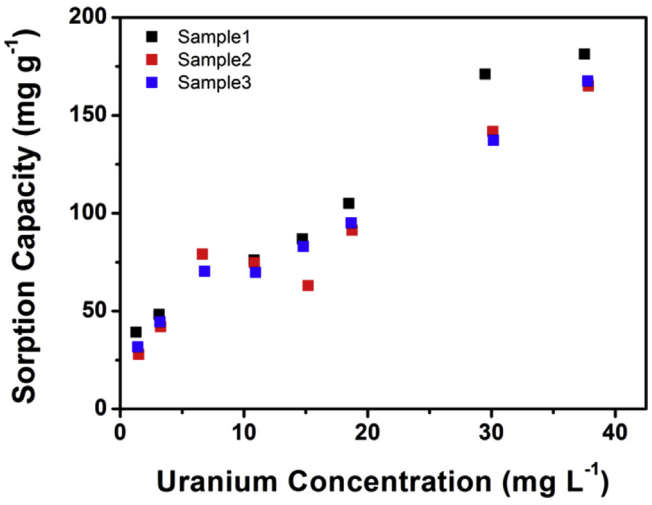

Fig. 9. The adsorption isotherm of different samples of Mn_3O_4@G towards uranyl ions at 298 K, pH = 5.0 and [I] = 0.01 M.

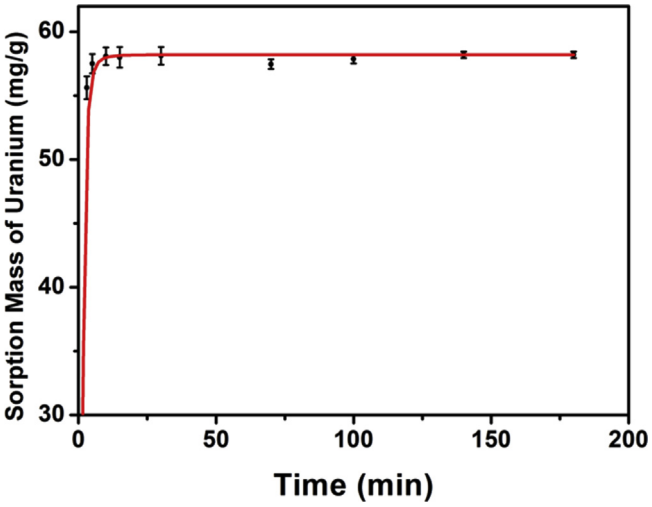

Fig. 10. Adsorption rate of Mn_3O_4@G ($[U]_{initial}$ = 31.2 mg L^{-1}, pH = 5, I = 0.01 M).

calculated to be 46.42 m^2 g^{-1}, nearly four times of the SSA of Mn_3O_4@G. A Type-B hysteresis loop is also observed, implying slit mesopores are also generated. As can be seen, G possesses more pores with the sizes of 1–5 nm, which the Mn_3O_4@G hardly possesses (Fig. 3f). The results above suggests that by removing the Mn_3O_4 nanoparticles from the nanocomposites, micropores and mesopores are generated inside the remaining RGO sheets. Thus, the Mn_3O_4 nanoparticles should occupy the spaces between the graphene sheets, namely, the Mn_3O_4@G nanocomposites have a unique sandwich-like structure.

3.4. Uranyl adsorption investigation

In previous reports, the RGO exhibits a poor adsorption ability towards uranyl ions, usually less than 50 mg g^{-1}, as most of the oxygen-containg groups have been removed. On the contrary, there are rich hydroxyl groups on the surface of Mn_3O_4 nanoparticles [25]. Thus, Mn_3O_4 nanoparticles play the role of absorbing uranyl ions, while the RGO play the role of carrying Mn_3O_4 nanoparticles and preventing them from aggregation.

Fig. 7a demonstrates the isotherm of Mn_3O_4@G adsorbing uranyl ions at 25 °C (pH = 5.0 ± 0.2 [I] (ionic strength) = 0.01 M). The adsorption curve of uranyl ions on Mn_3O_4@G is well described by Langmuir

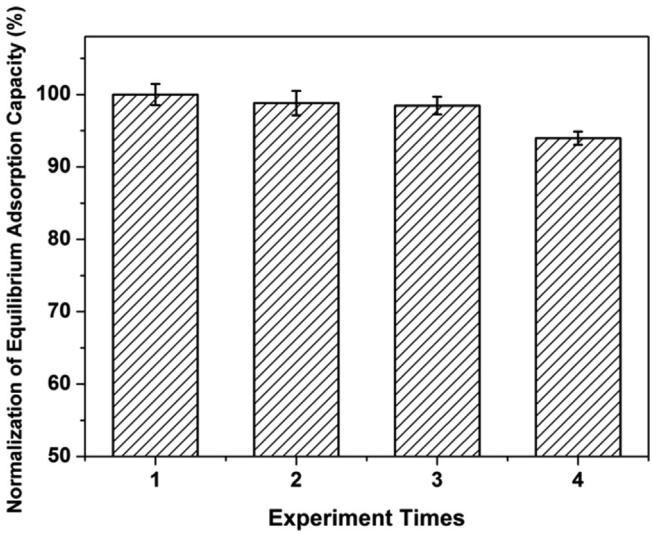

Fig. 11. Regeneration ability of Mn_3O_4@G ([U] = 31.2 mg L^{-1}, pH = 5, I = 0.01 M).

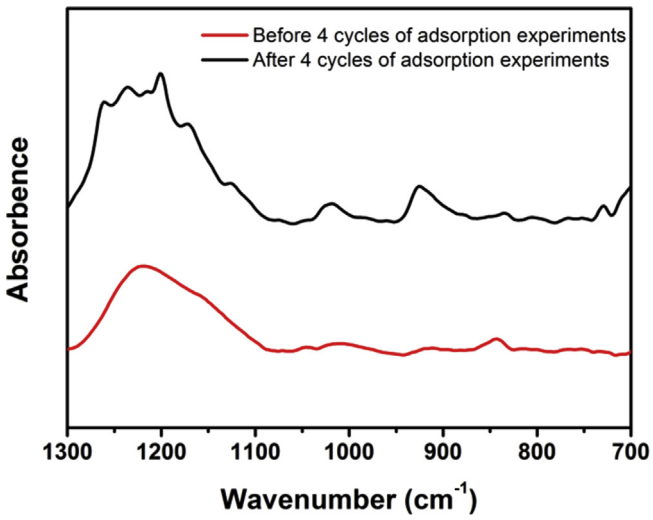

Fig. 12. The FTIR spectra of Mn_3O_4@G before and after 4 cycles of adsorption experiments.

isotherm. By applying the Langmuir Eq. (2), the maximum adsorption quantity, Q_{max}, is calculated to be 195.6 mg [U] g^{-1}, showing that Mn_3O_4@G is a reasonable adsorbent for the removal of uranyl ions. In the meanwhile, Q_{max} of the synthesized Mn_3O_4 is 170.1 mg [U] g^{-1} (Fig. 8). Given that the actual Mn_3O_4 content in Mn_3O_4@G is 68.2%, the Mn_3O_4 nanoparticles formed in the cracks between graphene sheets should possess larger active adsorption surface than that those formed in the free aqueous environment. Moreover, the adsorption ability is frepeatable (Fig. 9).

$$Q_e = \frac{kQ_{max}C_e}{1 + kC_e} \quad \text{Eq. (2)}$$

Furthermore, to evaluate the adaptability and stability of the Mn_3O_4@G as an adsorbent, the influences of pH and ionic strength were investigated. Mn_3O_4@G shows the highest adsorption quantity in the near-neutral condition of pH 6 (Fig. 4b). Like most other metallic oxides, too low or too high pH values goes against the adsorption of uranyl ions on Mn_3O_4@G. Meanwhile, the ionic strength seems to show indistinctive effect on the adsorption ability of Mn_3O_4@G. There are almost no changes of adsorption capacities when the ionic strength ranges from 0 M

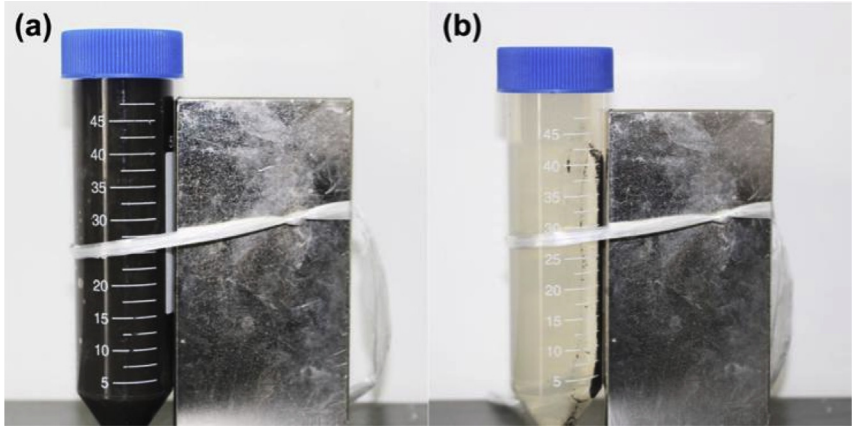

Fig. 13. Illustration of the magnetism of Mn_3O_4@G. a) suspension of Mn3O4@G, b)24 h later.

to 0.1 M, while a small decrease is observed on the increase of the ionic strength to 0.5 M. This is a typical phenomenon for the inner-sphere adsorption, which shows higher binding strength compared to the outer-sphere one.

To fully evaluate the adsorption ability of Mn_3O_4@G, the adsorption rate and the regeneration ability were also studied. As can be seen in Fig. 10, Mn_3O_4@G exhibits a rapid adsorption rate towards uranyl ions. It takes no more than 10 min to reach the adsorption equilibrium, showing the potential in urgent treatment of radioactive waste water pollution. However, the regeneration ability is not perfect. After four cycles of adsorption experiments, Mn_3O_4@G only remain 93.96 $\pm$ 0.90% of the initial equilibrium adsorption capacity (Fig. 11). The FTIR spectrum of the Mn_3O_4@G after four cycles adsorption experiments and washed by dilute HNO_3 shows new characteristic peaks at 920 cm^{-1} and 1020 cm^{-1} in the fingerprint region associated with the vibration of O=U=O, compared with the FTIR spectrum of the initial Mn_3O_4@G powders [26] (Fig. 12). The results indicate that there still residual uranyl ions absorbed on the surface of Mn_3O_4 even after washing. However, if the pH of the dilute HNO_3 decrease further, the Mn_3O_4 might suffer dissolution, which would also brought damages on the regeneration ability.

Besides, due to its magnetism, Mn_3O_4@G can be removed by magnetic field. As can be seen in Fig. 13, by locating a commercial magnet beside a plastic tube full of the concentrated Mn_3O_4@G suspension, after 24 h, most of the Mn3O4@G nanocomposites are attracted to the side of the magnet.

To sum up, Mn_3O_4@G is a kind of reasonable adsorbent for uranyl ions with high adsorption rate and special magnetism which made it easy to remove from the solution. Given the facility of preparation, Mn_3O_4@G exhibits a promising application as uranyl absorbent.

4. Conclusions

By modifying the post-treatment of Hummers' method to prepare chemical converted graphene, we synthesized a novel type of nanocomposites of reduced graphene oxide and Mn_3O_4 named as Mn_3O_4@G. The Mn element of the raw material is fully utilized, and the method achieves a better atom economy. Inside the Mn_3O_4@G nanocomposites, a large quantity of Mn_3O_4 nanoparticles distributed between graphene sheets, forming a unique sandwich-like structure. Importantly, the Mn_3O_4@G nanocomposites exhibit a potential adsorption ability of uranyl ions. The Mn_3O_4@G nanocomposites possess a reasonable maximum equilibrium adsorption quantity 195.6 mg [U] g^{-1} (298 K, pH = 5.0, and [I] = 0.01 M). By combining the magnetic material, Mn_3O_4 nanoparticles, and electric conductive material, reduced graphene oxide, Mn_3O_4@G would be potentially applied as electromagnetic shielding material. Furthermore, by adding other metallic ions into the reaction system of Hummers' method, other sandwich-like graphene/metal oxides nanocomposite could also be fabricated, which would extend the applications of the novel sandwich-like graphene composites.

Declarations

Author contribution statement

Yingru Li: Conceived and designed the experiments; Performed the experiments; Analyzed and interpreted the data; Wrote the paper.

Yiming Ren: Conceived and designed the experiments.

T Gai: Performed the experiments.

L Shao & H Tang: Analyzed and interpreted the data.

R Li, SL Yang, SF Wang & Q Wu: Contributed reagents, materials, analysis tools or data.

Funding statement

This work was supported by the Initiative Scientific Research Program of Materials Institute, CAEP (TP02201704), the Science Challenge Project (SCP, No. TZ20160040303) and the National Natural Science Foundation of China (21507118).

Competing interest statement

The authors declare no conflict of interest.

Additional information

No additional information is available for this paper.

References

[1] F. Fan, H. Ding, J. Bai, X.L. Wu, F.A. Lei, W. Tian, et al., Sorption of uranium (VI) from aqueous solution onto magnesium silicate hollow spheres, J. Radioanal. Nucl. Chem. 289 (2) (2011) 367–374.

[2] Y. Ren, R. Yang, L. Shao, H. Tang, S. Wang, J. Zhao, et al., The removal of aqueous uranium by SBA-15 modified with phosphoramide: a combined experimental and DFT study, RSC Adv. 6 (73) (2016) 68695–68704.

[3] Y. Ren, H. Tang, L. Shao, J. Zhong, M. Chu, R. Yang, et al., Theoretical study on complexation of U (VI) with ODA, IDA and TDA based on density functional theory, RSC Adv. 6 (52) (2016) 46467–46474.

[4] Y. Sun, J. Li, X. Wang, The retention of uranium and europium onto sepiolite investigated by macroscopic, spectroscopic and modeling techniques, Geochem. Cosmochim. Acta 140 (2014) 621–643.

[5] S. Ayata, S. Aydinci, M. Merdivan, G. Binzet, N. Kulcu, Sorption of uranium using silica gel with benzoylthiourea derivatives, J. Radioanal. Nucl. Chem. 285 (3) (2010) 525–529.
[6] J.R. Memon, K.R. Hallam, M.I. Bhanger, A.E. Turki, G.C. Allen, Evaluation of sorption of uranium onto metakaolin using X-ray photoelectron and Raman spectroscopies, Anal. Chim. Acta 631 (1) (2009) 69–73.
[7] H. Zeng, A. Singh, S. Basak, K.U. Ulrich, M. Sahu, P. Biswas, Nanoscale size effects on uranium (VI) adsorption to hematite, Environ. Sci. Technol. 43 (5) (2009) 1373–1378.
[8] S. Xie, Z. Chun, X. Zhou, J. Yang, X. Zhang, J. Wang, Removal of uranium (VI) from aqueous solution by adsorption of hematit, J. Environ. Radioact. 100 (2) (2009) 162–166.
[9] E.K. Lesher, J.F. Ranville, B.D. Honeyman, Analysis of pH dependent uranium (VI) sorption to nanoparticulate hematite by flow field-flow fractionation-inductively coupled plasma mass spectrometry, Environ. Sci. Technol. 43 (14) (2009) 5403–5409.
[10] J.D. Prikryl, A. Jain, D.R. Turner, R.T. Pabalan, UraniumVI sorption behavior on silicate mineral mixtures, J. Contam. Hydrol. 47 (2-4) (2001) 241–253.
[11] J.H. Jang, B.A. Dempsey, W.D. Burgos, Reduction of U (VI) by Fe (II) in the presence of hydrous ferric oxide and hematite: effects of solid transformation, surface coverage, and humic acid, Water Res. 42 (8-9) (2008) 2269–2277.
[12] D. Renock, M. Mueller, K. Yuan, R.C. Ewing, U. Becker, The energetics and kinetics of uranyl reduction on pyrite, hematite, and magnetite surfaces: a powder microelectrode study, Geochem. Cosmochim. Acta 118 (2013) 56–71.
[13] D.M. Singer, S.M. Chatman, E.S. Ilton, K.M. Rosso, J.F. Banfield, G.A. Waychunas, U (VI) sorption and reduction kinetics on the magnetite (111) surface, Environ. Sci. Technol. 46 (7) (2012) 3821–3830.
[14] J. Mukherjee, J. Ramkumar, R. Shukla, A.K. Tyagi, Sorption characteristics of nano manganese oxide: efficient sorbent for removal of metal ions from aqueous streams, J. Radioanal. Nucl. Chem. 297 (1) (2013) 49–57.
[15] Z. Wang, S.W. Lee, J.G. Catalano, J.S. Lezama-Pacheco, J.R. Bargar, B.M. Tebo, et al., Adsorption of uranium(VI) to manganese oxides: X-ray absorption spectroscopy and surface complexation modeling, Environ. Sci. Technol. 47 (2) (2013) 850–858.
[16] Z. Wang, W. Xiong, B.M. Tebo, D.E. Giamma, Oxidative UO_2 dissolution induced by soluble Mn (III), Environ. Sci. Technol. 48 (1) (2013) 289–298.
[17] S. Sambasivam, G.J. Li, J.H. Jeong, B.C. Choi, K.T. Lim, S.S. Kim, et al., Structural, optical, and magnetic properties of single-crystalline Mn_3O_4 nanowires, J. Nano Res. 14 (9) (2012) 1138.
[18] D. Li, R.B. Kaner, Graphene-based materials, Science 320 (5880) (2008) 1170–1171.
[19] A.K. Geim, Graphene: status and prospects, Science 324 (5934) (2009) 1530–1534.
[20] Y. Li, J. Chen, L. Huang, C. Li, G. Shi, "Pottery" of porous graphene materials, Adv. Electron. Mater. 1 (5) (2015) 1500004.
[21] S. Hidayat, F. Wang, T. Arbab, A. Shujaat, U. Zia, K. Zia Ul Haq, L. Yan, J. Hu, K. He, Electrochemical properties of controlled size Mn_3O_4 nanoparticles for supercapacitor applications, J. Nanosci. Nanotechnol. 18 (2018) 719–724.
[22] C. Liu, H. Song, C. Zhang, Y. Liu, C. Zhang, X. Nan, et al., Coherent Mn_3O_4-carbon nanocomposites with enhanced energy-storage capacitance, Nano. Res. 8 (10) (2015) 3372–3383.
[23] Z.W. Chen, J.K.L. Lai, C.H. Shek, Nucleation site and mechanism leading to growth of bulk-quantity Mn_3O_4 nanorods, Appl. Phys. Lett. 86 (18) (2005) 181911.
[24] K.N. Kudin, B. Ozbas, H.C. Schniepp, R.K. Prud'Homme, I.A. Aksay, R. Car, Raman spectra of graphite oxide and functionalized graphene sheets, Nano Lett. 8 (1) (2008) 36–41.
[25] Z. Li, F. Chen, L. Yuan, Y. Liu, Y. Zhao, Z. Chai, W. Shi, Uranium(VI) adsorption on graphene oxide nanosheets from aqueous solutions, Chem. Eng. J. 210 (2012) 539–546.
[26] Y. Ren, Q. Wu, J. Zhong, Z. Qin, L. Shao, H. Tang, C. Kong, Y. Li, Exploring uranyl/salicylate/hematite binary and ternary complexes by attenuated-total-reflection infrared spectroscopy, Chemistry 3 (17) (2018) 4570–4575.